Proceedings of NANO2005
ASME Integrated Nanosystems: Design, Synthesis & Applications
September 14-16, 2005 Berkeley, California, USA

NANO2005-87074-DRAFT

COMPRESSIVE PROPERTIES OF DENSE VERTICALLY ALIGNED MULTI-WALLED CARBON NANOTUBE ARRAYS

Tao Tong [*], Yang Zhao [†], Lance Delzeit [§], Carmel Majidi [‡], Richard E. Groff [‡], Pramod Reddy[‡‡], Arun Majumdar[* **] [1], Ali Kashani [†], and M. Meyyappan [§]

[*] Department of Mechanical Engineering, UC Berkeley, Berkeley, CA 94720
[†] Atlas Scientific, Inc., San Jose, CA 95120
[§] NASA Ames Research Center, Moffett Field, CA 94035
[‡] Department of Electrical Engineering and Computer Science, UC Berkeley, Berkeley, CA 94720
[‡‡] Applied Science and Technology, UC Berkeley, Berkely, CA 94720
[**] Materials Sciences Division, Lawrence Berkeley National Laboratory, Berkeley, CA 94720

ABSTRACT

We performed compression tests to dense vertically aligned multi-walled carbon nanotube (MWCNT) arrays using a home-made mini-loading test platform. Effective spring constants and compressive moduli of the MWCNT arrays are derived from the force-displacement relations. The effective compressive moduli are found to be ~0.2 MPa independent of nanotube lengths. A simplified continuum mechanics model is developed to explain the experimental observations.

INTRODUCTION

While the major research interests of mechanical properties of carbon nanotubes lie in the measurement of a single nanotube [1,2] or dispersed nanotubes in composite materials [3], mechanical properties of the carbon nanotubes in the form of a dense vertically aligned array has been largely neglected yet. Recently, Kinoshita *et al*. [4] studied the micro-tribological properties of vertically aligned MWCNT array films (~6 μm long); Qi *et al*. [5] studied the bending properties of short vertically aligned MWCNT array of a few μm long using nanoindentation; Pan *et al*. [6] performed tensile tests on long (~1 mm) MWCNT ropes to study tensile modulus and breaking strength. However, compressive properties of relatively long MWCNT arrays are still missing in the literature. In this study, we developed a mini-loading test platform and conducted compression tests to MWCNT arrays with various array heights.

EXPERIMENT

The MWCNTs used in this work were grown on Si wafer by thermal CVD with iron (Fe) as catalyst. Ethylene was used as the feedstock and the growth temperature is about 750 ^{o}C. Detailed discussions on nanotube growth are seen in Ref. [7]. The resulted MWCNTs have diameters ranging from 20-30 nm and an aerial density ~10^{10} tubes/cm^2. Depending on the growth time, the MWCNT arrays have lengths ranging from a few to more than 500 μm. Typical MWCNT array pictures are shown in Fig. 1.

[1] Corresponding author – Email: majumdar@me.berkeley.edu

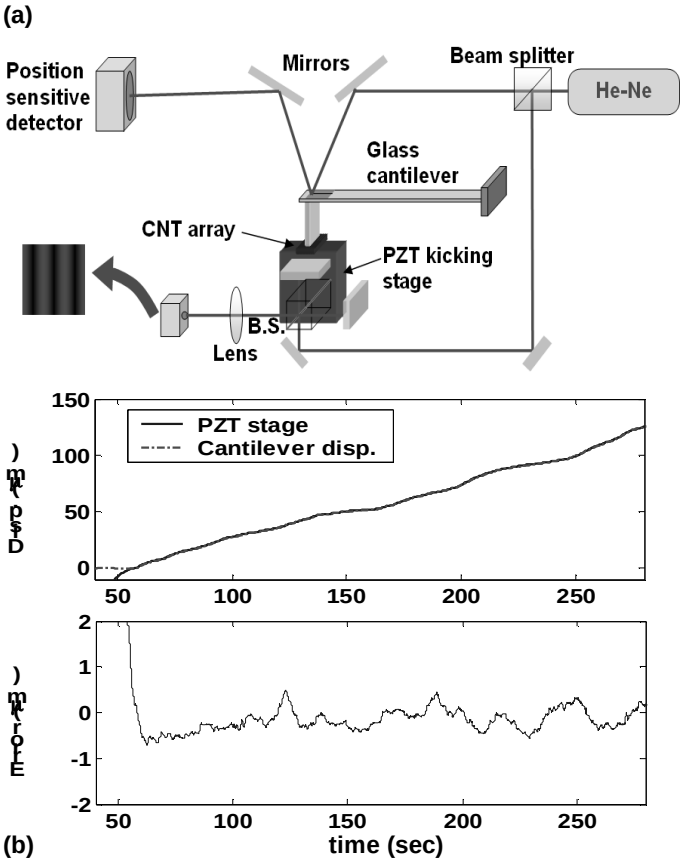

Fig. 2 (a) Loading test platform based on optical detection. (b) Calibration curve of the stage.

A mini-loading platform for tensile and compressive tests based on optical detection techniques was built with an overall displacement resolution less than 1 μm and force resolution ~1 milli-Newton (mN). Shown in the schematic of Fig. 2(a), the loading section has two parts: a glass cantilever of ~6 cm long from above and a piezoelectric (PZT) kicking stage from below. The glass cantilever acts as a displacement sensor and a force sensor. The laser beam reflected from the tip of the cantilever is read by a four quadrant position sensitive detector (PSD). From the geometry of the setup, cantilever tip displacement can be determined, and thus the force, given the knowledge of the spring constant of the cantilever. The loading process is driven by the PZT kicking stage. The current design of the kicking stage is almost a replica of Silveira and Marohn's design [8]. A sawtooth electrical signal with maximum amplitude of 10 Vpp at a frequency of 666 Hz is used to drive the PZT stage. A Michelson interferometer was built on the stage to track its displacement. Currently, the PZT stage can deliver a travel range over 1 mm with a resolution of 10 nm and provide a driving force of ~4-5 grams, which can be easily raised with a more powerful signal generator. Figure 2(b) shows the calibration curve of the platform, where the PZT stage pushes up the cantilever tip rigidly. In the displacement figure, the blue solid curve represents the PZT stage movement with respect to time and the red dashed curve represents the tip displacement of the cantilever. The difference in the initial section of the curve is before the PZT stage came into contact with the cantilever. The error between the two displaements, as seen in the lower figure, is generally within ±0.5 μm.

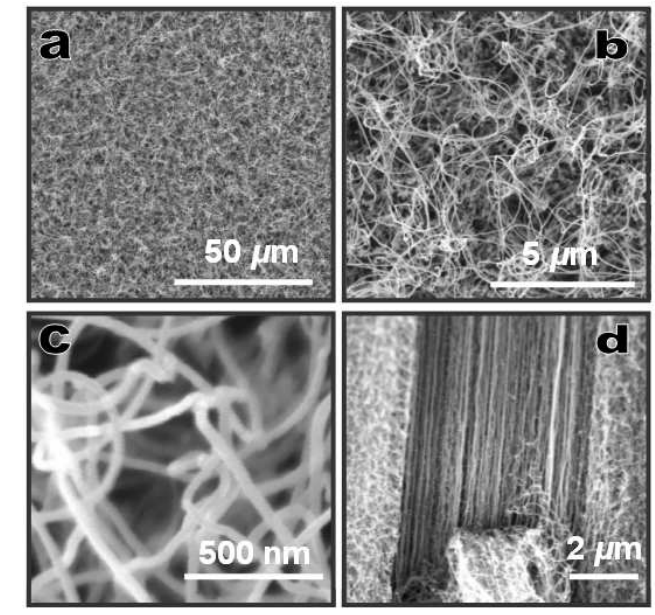

Fig. 1 Scanning electron microscope (SEM) pictures of MWCNT arrays. (a-c) Top view with increasing magnification. (d) Side view of a sample where a patch of outer layer being peeled off, showing vertical alignment of the tubes.

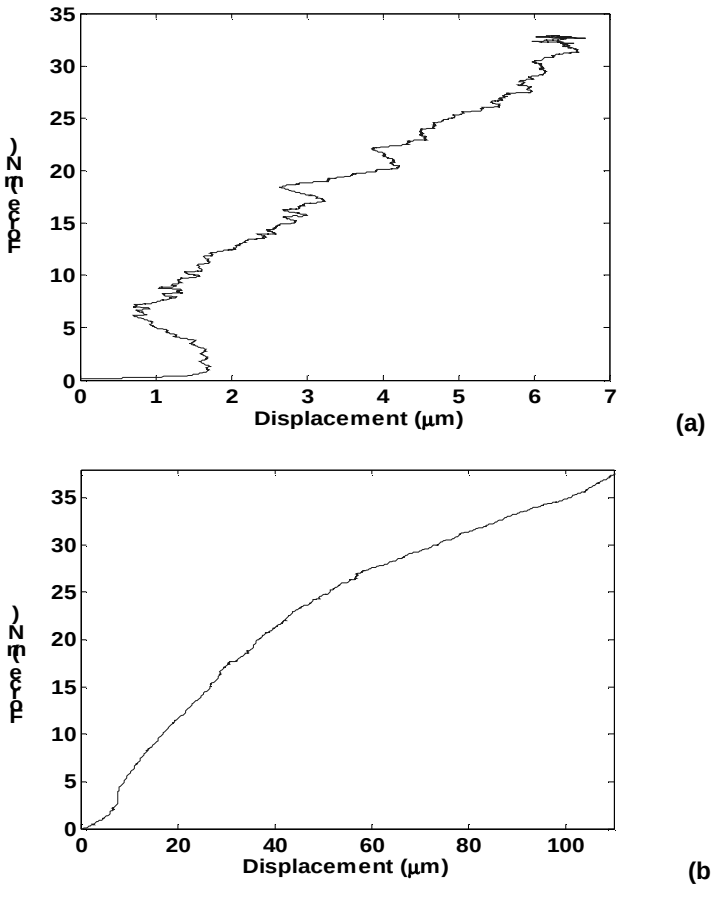

Fig. 3 Force-displacement curves of compression tests with (a) 40 μm and (b) 500 μm long MWCNT arrays.

During the compression test, a rigid surface with known area is pressed against a MWCNT array surface in the vertical direction. Force-displacement relation is recorded during the process. Based on the force-displacement curve, the effective spring constant can be obtained, and further the effective compressive modulus of the array derived.

RESULTS AND DISCUSSION

Force-displacement curves of 40 μm and 500 μm long MWCNT arrays are shown in Fig. 3. The "swing backs" in the initial section and the middle section of the 40 μm curve might result from measurement noise. For the same contact surface (500μm × 2mm) of the side of a rigid quartz plate, the spring constant of the MWCNT array with such contact area is ~4200 N/m for the 40 μm long sample, and varies from 550 to 200 N/m for the 500 μm sample for loading displacements from less than 40 μm to more than 100 μm. Converted to the language of strain-stress, the average effective compressive moduli (E_{eff} = $(F/Area)/(\Delta L/L)$) are ~0.23 MPa for the 40 μm long sample and ~0.27-0.18 MPa for the 500 μm sample.

For the two samples tested with 10 times difference in tube lengths, the effective moduli lie in the same range and the spring constants almost vary inversely proportional to tube lengths (L^{-1}). The effective compressive modulus of the MWCNT array is much lower than the intrinsic Young's modulus of a single carbon nanotube (several hundred GPa to more than 1 TPa), and even much lower than those of ordinary polymers (~ several hundred MPa to a few GPa). It is clear that the low compressive modulus of the array is due to the bending of the very-high aspect ratio of nanotubes, so the compressive modulus of the array is more of a structural property rather than a property of the nanotube itself.

To qualitatively understand the observed low compressive modulus of the array and linear dependence of the spring constant, we consider a simplified mechanical model of the MWCNT array, where the surface entanglement of the tubes and tube-tube van der Waals interactions are neglected. As shown in Fig. 4(a), each nanotube is modeled as an elastica of length L, elastic modulus E, and area moment of inertia I, subject to a compressive load, F, that acts downward on the tip. When F exceeds the critical value $F_{cr} = \pi^2 EI/4L^2$ the nanotube buckles, causing the tip to deflect by an angle α. Following from the equations of motion for an elastica, the normalized vertical displacement or strain of the tip can be expressed as [9]

$$\frac{\Delta}{L} = 2 - \frac{4}{\pi} E(p) \sqrt{\frac{F_{cr}}{F}} . \qquad (1)$$

where the modulus $p = \sin(\alpha/2)$ is the solution to

$$K(p) = \frac{\pi}{2} \sqrt{\frac{F}{F_{cr}}} . \qquad (2)$$

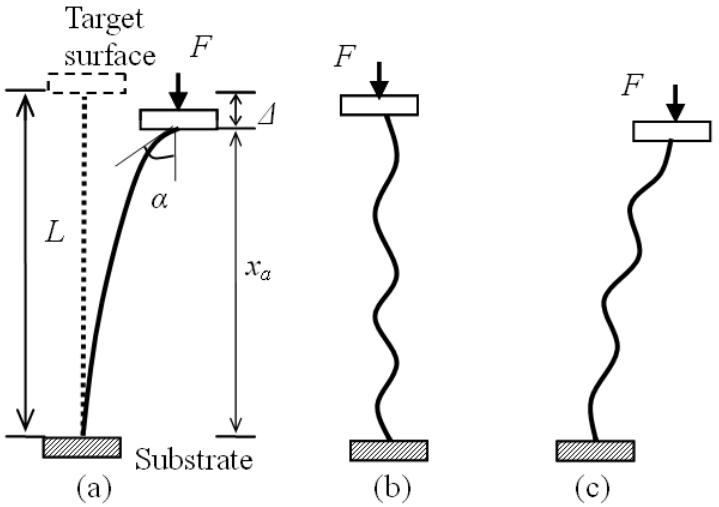

Fig. 4 Structural model of the nanotubes.

Here, the functions $K(\bullet)$ and $E(\bullet)$ are the complete elliptic integrals of the first and second kind, respectively. For α small, $E(p) \approx (\pi/2)(1 - p^2/4)$ and $K(p) \approx (\pi/2)(1 + p^2/4)$ [10]. Substituting these expressions into the above equations and solving for the normalized load,

$$\frac{F}{F_{cr}} = 16\left(4 - \frac{\Delta}{L}\right)^{-2} . \qquad (3)$$

Taking the derivative of the force with respect to Δ, we obtain the local spring constant. For $\Delta/L < 0.2$, this is approximately equal to

$$k_{local} = k_0 = \frac{F_{cr}}{2L} = \frac{\pi^2 EI}{8L^3} . \qquad (4)$$

A numerical evaluation without approximation gives about 20% larger spring constant than above considering an average strain of 10%. For E = 200 GPa, $I = \pi(D^4 - d^4)/64$, where the outer diameter D = 25 nm and inner diameter d = 10 nm, a density of 10^{10} nanotubes/cm^2, and apparent contact area of 500μm × 2mm, the spring constant is calculated to be ~8.6 N/m for the 40 μm array and another 1000 times smaller for the 500 μm sample. Notice, however, that the L^{-3} dependence of the spring constant is contradictory to the observed L^{-1} dependence.

It is observed under the SEM that the long nanotubes are inherently wavy along its tube axis. As seen in Fig.1(d), nanotubes at the outer layer of the array are very curly; even the much straighter inner nanotubes show this wavy characteristic. Under compressive loading, the buckling of the nanotube may not just stay in the fundamental mode, but rather at a higher nth mode (Fig.4(b)) containing n waves from end to tip (the fundamental mode contains *1/4* wave with the assumed boundary conditions), where n should lie between the fundamental value and the number of natural wrinkles of the nanotube considering the natural wrinkles act as a guide for the buckling. Assuming the nanotube takes an evenly distributed sinusoidal shape with a period $p=L/n$.

Since a period of the nanotube can be regarded as four sections of that in Fig.4(a) connected in series, it follows from Equ. (4) that the equivalent local spring constant of a nanotube of the *n*th mode is:

$$k_n = \frac{1}{4n}\frac{\pi^2 EI}{8(L/4n)^3} = 16n^2 k_0 . \qquad (5)$$

To come up with a prediction consistent with the experimental value of the 40 μm sample, we get n ≈ 5.5, and for 500 μm sample, n ≈ 82, roughly proportional to tube lengths. This buckling mode should be regarded as a statistical average of the array. Considering the many approximations used in the model, the actual mode number might be quite different from the prediction and awaits direct experimental verification. If the buckling mode is regarded as a characteristic of the nanotube, the average period *p* should be independent of the nanotube length or *n* is linearly proportional to the nanotube length. Thus naturally comes the L^{-1} dependence of the spring constant with nanotube length, which is consistent with experiment.

Considering the buckling model, there are no observed threshold loadings in the experiment. This might be due to the uneven height distribution of the nanotubes in the array that make it extremely hard to observe critical loading on a tube-tube basis. From the force-displacement curve of the 500 μm sample in Fig.3(b), it shows after an initially relatively flat region before 8 μm of displacement, the force hikes up with the maximum slope up to 50-60 μm, and then the slope softens at larger displacements indicating possibly mixed mode buckling and/or bending due to partially shear loading (Fig.4(c)).

CONCLUSION

Compression tests have been performed to MWCNT arrays with tube lengths of 40 μm and 500 μm on a home-made mini-loading test platform. The effective compressive modulus of the MWCNT array is found to be ~0.2 MPa, much independent of nanotube length. A simplified continuum mechanical model based on buckling of the nanotubes is put forth to compare with the experimental values and also try to explain the apparent independence to nanotube length of the compressive modulus.

ACKNOWLEDGMENTS

The authors gratefully acknowledge the financial support for this work from NASA SBIR program 18521.

REFERENCES

[1] M.F. Yu, O. Lourie, M.J. Dyer, K. Moloni, T.F. Kelly, and R.S. Ruoff, Strength and Breaking Mechanism of Multiwalled Carbon Nanotubes Under Tensile Load, Science, 287 (2000) 637-640.

[2] Y.Q. Zhang, G.R. Liu, and J.S. Wang, Small-Scale Effects on Buckling of Multiwalled Carbon Nanotubes Under Axial Compression, Physical Review B, 70 (2004) .

[3] E.T. Thostenson and T.W. Chou, Nanotube Buckling in Aligned Multi-Wall Carbon Nanotube Composites, Carbon, 42 (2004) 3015-3018.

[4] H. Kinoshita, I. Kume, M. Tagawa, and N. Ohmae, High Friction of a Vertically Aligned Carbon-Nanotube Film in Microtribology, Applied Physics Letters, 85 (2004) 2780-2781.

[5] H.J. Qi, K.B.K. Teo, K.K.S. Lau, M.C. Boyce, W.I. Milne, J. Robertson, and K.K. Gleason, Determination of Mechanical Properties of Carbon Nanotubes and Vertically Aligned Carbon Nanotube Forests Using Nanoindentation, Journal of the Mechanics and Physics of Solids, 51 (2003) 2213-2237.

[6] Z.W. Pan, S.S. Xie, L. Lu, B.H. Chang, L.F. Sun, W.Y. Zhou, G. Wang, and D.L. Zhang, Tensile Tests of Ropes of Very Long Aligned Multiwall Carbon Nanotubes, Applied Physics Letters, 74 (1999) 3152-3154.

[7] L. Delzeit, C.V. Nguyen, B. Chen, R. Stevens, A. Cassell, J. Han, and M. Meyyappan, Multiwalled Carbon Nanotubes by Chemical Vapor Deposition Using Multilayered Metal Catalysts, Journal of Physical Chemistry B, 106 (2002) 5629-5635.

[8] W.R. Silveira and J.A. Marohn, A Vertical Inertial Coarse Approach for Variable Temperature Scanned Probe Microscopy, Review of Scientific Instruments, 74 (2003) 267-269.

[9] S.P. Timoshenko and J.M. Gere, Theory of Elastic Stability, McGraw-Hill, Inc., (1961) .

[10] P.F. Byrd and M.D. Friedman, Handbook of Elliptic Integrals for Engineers and Scientists, Springer-Verlag, (1971) .